A Preliminary Study toward Consistent Soil Moisture from AMSR2

ROBERT M. PARINUSSA

Earth and Climate Cluster, VU University Amsterdam, Amsterdam, Netherlands, and the School of Civil and Environmental Engineering, University of New South Wales, Sydney, New South Wales, Australia

THOMAS R. H. HOLMES

Hydrology and Remote Sensing Laboratory, Agricultural Research Services, U.S. Department of Agriculture, Beltsville, and Science Systems and Applications, Lanham, Maryland

NIKO WANDERS

Department of Physical Geography, Utrecht University, Utrecht, Netherlands

WOUTER A. DORIGO

Department of Geodesy and Geo-Information, Vienna University of Technology, Vienna, Austria

RICHARD A. M. DE JEU

Earth and Climate Cluster, VU University Amsterdam, Amsterdam, Netherlands

(Manuscript received 9 December 2013, in final form 17 November 2014)

ABSTRACT

A preliminary study toward consistent soil moisture products from the Advanced Microwave Scanning Radiometer 2 (AMSR2) is presented. Its predecessor, the Advanced Microwave Scanning Radiometer for Earth Observing System (AMSR-E), has provided Earth scientists with a consistent and continuous global soil moisture dataset. A major challenge remains to achieve synergy between these soil moisture datasets, which is hampered by the lack of an overlapping observation period of the sensors. Here, observations of the multifrequency microwave radiometer on board the Tropical Rainfall Measuring Mission (TRMM) satellite were used to improve consistency between AMSR-E and AMSR2. Several scenarios to achieve synergy between the AMSR-E and AMSR2 soil moisture products were evaluated. The novel soil moisture retrievals from C-band observations, a frequency band that is lacking on board the TRMM satellite, are also presented. A global comparison of soil moisture retrievals against ERA-Interim soil moisture demonstrates the need for an intercalibration procedure. Several different scenarios based on filtering were tested, and the impact on the soil moisture retrievals was evaluated against two independent reference soil moisture datasets (reanalysis and in situ soil moisture) that cover both individual observation periods of the AMSR-E and AMSR2 sensors. Results show a high degree of consistency between both satellite products and two independent reference products for the soil moisture products retrieved from X-band observations. Care should be taken in the interpretation of the presented soil moisture products, and future research is needed to further align the AMSR2 and AMSR-E sensor calibrations.

1. Introduction

The Advanced Microwave Scanning Radiometer for Earth Observing System (AMSR-E) has provided Earth scientists with valuable observational data on Earth's climate system for almost a decade. AMSR-E was one of the six Earth-observing instruments on board the National Aeronautics and Space Administration (NASA) *Aqua* satellite, a mission specifically designed to provide observational information on many components of the hydrological cycle. The *Aqua* satellite was launched on 4 May 2002 and is currently still in orbit. However, AMSR-E was switched off on 4 October 2011 because of

Corresponding author address: R. M. Parinussa, University of New South Wales, Vallentine Annexe (H22), Room 127, Sydney NSW 2052, Australia.
E-mail: r.parinussa@unsw.edu.au

DOI: 10.1175/JHM-D-13-0200.1

rotation problems with its antenna. The Advanced Microwave Scanning Radiometer 2 (AMSR2) is intended to extend the valuable legacy of AMSR-E and shares a similar design with its predecessor. It was improved based on general technical development and experience with AMSR-E. For example, a neighboring C-band frequency was added to AMSR2 in order to improve radio frequency interference (RFI) mitigation. In January 2013, the Japan Aerospace Exploration Agency (JAXA) started offering brightness temperature T_b observations from the AMSR2 radiometer on board the *Global Change Observation Mission 1–Water* (*GCOM-W1*) that was launched on 17 May 2012.

A major challenge for both satellite engineers and Earth scientists is providing consistency between the products of AMSR-E and AMSR2. Satellite engineers must provide consistent brightness temperature products, while Earth scientists must provide consistent geophysical parameters of our atmosphere, oceans, and/or land surfaces. The absence of a common observation period makes consistent radiometer calibration increasingly difficult, thus directly impacting consistency in the retrieved geophysical parameters. A possible solution is to use observations from other passive microwave radiometers, such as the Tropical Rainfall Measuring Mission (TRMM) Microwave Imager (TMI). The TMI is a multifrequency microwave radiometer on board the TRMM satellite. In contrast to the polar-orbiting *Aqua* and *GCOM-W1* satellites, TRMM is in near-equatorial orbit. A result of these divergent orbit types is that the TMI record overlaps with both AMSR sensors at recurring times within their respective observation periods. A downside of the TMI sensor compared to the others (AMSR-E and AMSR2) is the lack of observations in the low C-band frequency, as these observations have the most sensitivity to soil moisture. Here, we aim for consistency between surface soil moisture retrievals from the AMSR-E and AMSR2 sensor from observations in the X band. Novel surface soil moisture retrievals from both AMSR2 C-band frequency channels were also presented and compared against the two independent reference soil moisture datasets (reanalysis and in situ soil moisture).

Surface soil moisture plays an important role in many water- and energy-related processes. Since global soil moisture products from satellite observations became available more than a decade ago, several research applications have shown the importance of this parameter. Satellite soil moisture data have been used to improve weather predictions (e.g., Loew et al. 2009; Bisselink et al. 2011), hydrological model calibration (e.g., Wanders et al. 2014a), and runoff predictions (e.g., Beck et al. 2009; Brocca et al. 2010; Wanders et al. 2014b); to enhance our knowledge on land–atmosphere interaction (e.g., Jung et al. 2010; Taylor et al. 2012; Miralles et al. 2014); and to improve landslide predictions (Brocca et al. 2012). The Global Climate Observing System (GCOS) listed soil moisture as an essential climate variable (ECV) in 2010 (GCOS 2010), which motivated the European Space Agency (ESA) to incorporate this variable in their Climate Change Initiative (CCI) program (Hollmann et al. 2013). AMSR-E plays a prominent role in the CCI for soil moisture (Liu et al. 2012; Wagner et al. 2012), and the production of soil moisture from AMSR2 can potentially fill the gap left by AMSR-E.

A number of algorithms (e.g., Njoku et al. 2003; Jackson et al. 2004; Owe et al. 2008; Jones et al. 2010) to retrieve global soil moisture products from AMSR-E observations exist. One of the more intensively used soil moisture products is based on the Land Parameter Retrieval Model (LPRM; Owe et al. 2008). This model is entirely driven by passive microwave observations and is based on a simple radiative transfer equation to obtain soil moisture and vegetation optical depth simultaneously. LPRM partitions the microwave observation into its respective soil and vegetation emission components (Meesters et al. 2005) based on the horizontal H and vertical V polarized brightness temperatures (either C or X band). The LPRM uses an external algorithm to estimate land surface temperature (Holmes et al. 2009). In this study, the focus is on the soil moisture output of the LPRM; however, the vegetation optical depth and land surface temperature could be analyzed similarly.

This paper is organized as follows. In section 2, we focus on the brightness temperature observations obtained by remote sensing. An overview of the various multifrequency passive microwave sensors used in this study is given, followed by an intercalibration procedure and information on man-made contamination (i.e., RFI). The switch to geophysical land surface products is made in section 3, where the datasets used in this study, as well as the retrieval algorithm, are detailed. Section 4 shows a comparison between the soil moisture products, including a comparison to reanalysis data, and ground-based observations and examines a case study of anomalies in Australia. Finally, section 5 describes the conclusions and outlook of future research.

2. Multifrequency passive microwave observations

a. Passive microwave observations relevant for this study

Microwave observations are sensitive to water molecules and therefore play an important role in observing the varying phases and quantities of water in both time and space. AMSR-E was a long-serving Earth observation

TABLE 1. Specifications of the AMSR-E, AMSR2, and TMI microwave sensors that are relevant for this study.

Parameter	AMSR-E	AMSR2	TMI
Frequencies (GHz)	6.925, 10.65, and 36.5	6.925, 7.3, 10.65, and 36.5	10.7 and 37.0
Bandwidth (GHz)	0.35, 0.10, and 1.0	0.35, 0.35, 0.10, and 1.0	0.10 and 2.0
Polarization (all frequencies)	*H* and *V*	*H* and *V*	*H* and *V*
Incidence angle (all frequencies)	55°	55°	52.8°
Processing version (swath)	V003: Maturity details V12 Stage 1	V1.1	V7
Sample sized footprints (km)	43 × 74 for C band 30 × 51 for X band 8 × 14 for Ka band	35 × 61 for C band 35 × 61 for C band 24 × 41 for X band 7 × 12 for Ka band	72 × 43 for X band 18 × 10 for Ka band
Altitude (km)	705	700	400
Swath width (km)	1445	1450	878
Ascending orbit	1330 LT	1330 LT	Equatorial orbit
Descending orbit	0130 LT	0130 LT	Equatorial orbit
Data period	From May 2002 to Oct 2011	From Jul 2012 to present	From Dec 1998 to present

sensor in this scope. Originally, AMSR-E was planned to have an identical twin sensor on board the *Advanced Earth Observation Satellite II* (*ADEOS II*); however, this sensor broke down because of a power failure after 9 months. Observations of AMSR-E covered a range of microwave frequencies and provided Earth scientists with valuable observational data on precipitation, water vapor, sea ice extent, sea surface temperature, and soil moisture. AMSR-E was a cooperative effort between JAXA and NASA, which was extended over recent years in order to further develop this successful concept, leading to AMSR2 on board the *GCOM-W1* satellite that was launched on 17 May 2012.

The longest passive microwave data record from a single satellite platform is observed by the TMI. The TRMM satellite is also a cooperative effort between JAXA and NASA; it was specifically designed to study tropical rainfall, including its diurnal variation. TRMM was launched on 27 November 1997 and was originally designed for a 3–5-yr lifetime. However, it is currently still in operation, providing Earth scientists with valuable observational data. To capture the diurnal variability, the TRMM satellite is in (near) equatorial orbit covering the latitudes between 38°N and 38°S, therefore having variable overpass times throughout the day. The sensor scans the Earth's surface in nine different channels with 16 orbits per day. A downside of the TMI sensor compared to the others (AMSR-E and AMSR2) is the lack of observations in the low C-band frequency, as these observations have more sensitivity to soil moisture.

The WindSat multifrequency polarimetric microwave radiometer on board the *Coriolis* satellite (Gaiser et al. 2004) could potentially be useful for intercalibration purposes of this low C-band frequency. AMSR-E and WindSat share a long (8+ years) overlapping observation period and were used consistently in several studies (e.g., Parinussa et al. 2011a, 2012). Unfortunately, the distribution of WindSat data was terminated at the end of July 2012, leading to an insufficient overlapping observation period with AMSR2. In this study, all passive microwave observations were resampled to a daily 0.25° × 0.25° regular grid.

As mentioned earlier, low-frequency passive microwave observations (L-band frequency) have the most sensitivity to soil moisture, which is the reason that dedicated soil moisture missions like the current Soil Moisture Ocean Salinity (SMOS; Kerr et al. 2010) and future Soil Moisture Active Passive (SMAP; Entekhabi et al. 2010) have an L-band radiometer as the core instrument. The multifrequency passive microwave radiometers of AMSR-E and AMSR2 lack this low-frequency channel but instead have the advantage to leverage multichannel observations to estimate additional land surface parameters (Parinussa et al. 2011a). Sensor and satellite characteristics relevant for this study are given in Table 1. For more detailed information on the *Aqua* AMSR-E and the *GCOM-W1* AMSR2 sensors, the reader is referred to Imaoka et al. (2010), and for TMI the reader is referred to Kummerow et al. (1998).

b. Radiometer intercalibration

On a regular basis, the TMI sensor observes/observed the same regions at the same moment in time as the AMSR2 and AMSR-E sensors. The TRMM satellite is in a near-equatorial orbit (38°N–38°S), resulting in overlap at regular intervals throughout the year. As a result, the concurrent observations between TMI and the other two sensors (AMSR-E and AMSR2) cover the entire range required for the retrieval of soil moisture. Figure 1 shows these concurrent observations over land for the AMSR-E–TMI (cyan asterisks; blue regression line) and AMSR2–TMI (orange asterisks; red regression

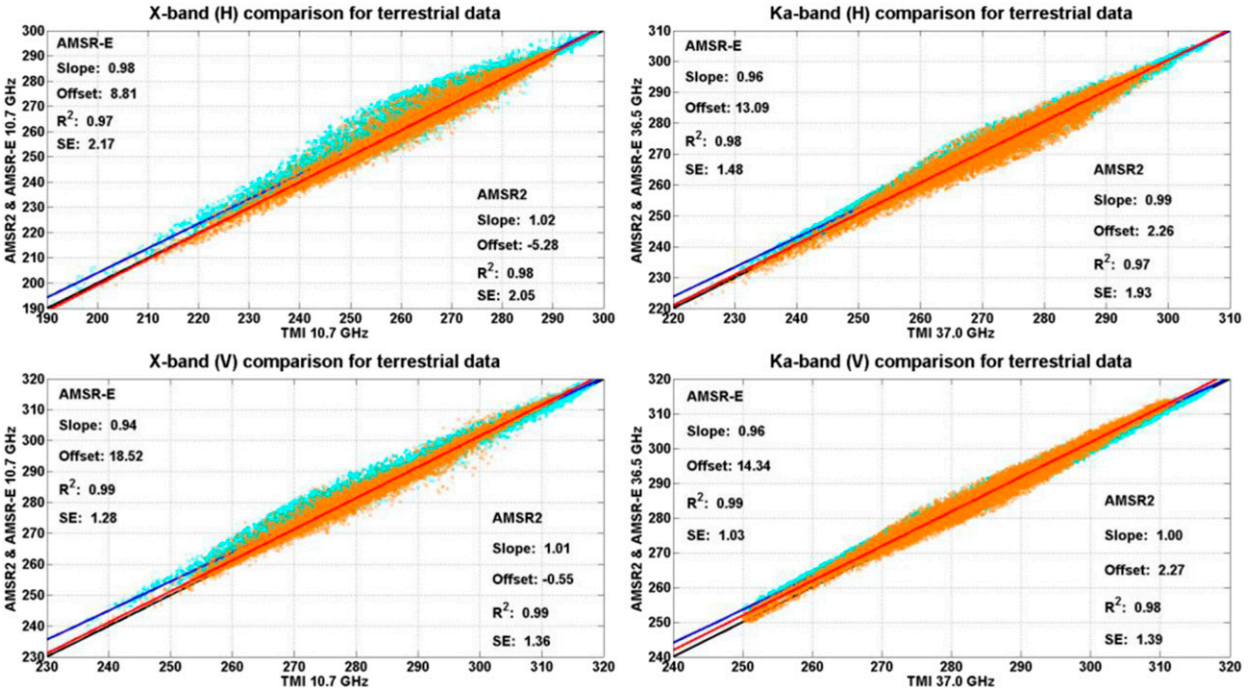

FIG. 1. The linear relations that can be used to transfer the calibration of the AMSR-E sensor into the future and to apply these relations to the AMSR2 sensor, all by means of the TMI sensor. In the (left) X- and (right) Ka-band frequencies, (top) *H* and (bottom) *V* polarization are presented. The symbols represent the individual observation pairs for AMSR2 (orange asterisks) and AMSR-E (cyan asterisks) whereas the lines (red and blue, respectively) represent their linear regressions.

line) sensor combinations, which were extracted for intercalibration purposes. The concurrent observations for the AMSR-E–TMI and AMSR2–TMI sensor pairs at horizontal (top) and vertical (bottom) polarization are presented in the X-band (left) and Ka-band (right) frequencies. All concurrent datasets were presented after the masking of outliers based on a standard Cook's distance filter (Cook 1977).

Although the TMI, AMSR-E, and AMSR2 sensors are comparable, differences in the observed brightness temperatures occur because of different calibration procedures and because of small differences in sensor specifications (e.g., center frequency, bandwidth, and incidence angle; Table 1). Parinussa et al. (2012) proposed an adjusting step for brightness temperature observations in order to reach consistency between AMSR-E and WindSat, accounting for these sensor differences as well as the different calibration procedures. It is emphasized that the AMSR-E and WindSat sensor have an 8-yr overlapping observation period, whereas AMSR2 and WindSat only share a single month of overlapping observation. Here, we build on the study of Parinussa et al. (2012), with the essential modification of using the TMI sensors as a transfer reference between the AMSR-E and AMSR2 sensors that do not have a direct overlap period. As a consequence, observations in the C-band frequency are not considered in the intercalibration procedure.

Not all concurrent brightness temperature observations over land as presented in Fig. 1 ultimately need to be used for the intercalibration. We considered three different intercalibration scenarios, roughly indicated with no intercalibration procedure, strictest filtering, and the use of all concurrent brightness temperature observations over land. The first scenario represents the baseline in which the LPRM retrieval algorithm is directly applied to the AMSR2 as provided by the data center without any additional sensor calibration considerations. This scenario was applied to the three lowest-frequency channels of the AMSR2 sensor, both C-band channels (6.9 and 7.3 GHz), and the X-band channel (10.7 GHz). The second scenario makes use of the strictest masking procedure that filters the brightness temperature pairs based on several criteria. Possible frozen and snowy conditions were filtered after the application of the land surface temperature algorithm (Holmes et al. 2009), including a 4 K bias that was found by Holmes et al. (2009) after comparing these outcomes against a radiative transfer model. Additional filtering was applied by using the standard deviation of the mean brightness temperature observation within a 0.25° × 0.25° grid cell from the vertically polarized Ka-band

observations. Holmes et al. (2013) found that an exceedance of such standard deviation by 0.7 K could be linked to frozen and snowy conditions and additionally to heterogeneous land cover, open water bodies, and active precipitation events. Another filtering condition that was based on sample sizes was taken from Holmes et al. (2013). Pixels in which the sample size to calculate the standard deviation was smaller than the median over the entire time series were also removed for further analysis. Finally, the fraction of open water data that is offered together with the brightness temperature products was set to its maximum value; therefore, only the observations taken over land according to these internal data were considered in this scenario. In contrast, the final scenario uses all terrestrial brightness temperature observations to extract the linear regressions.

The red (AMSR2) and blue (AMSR-E) regression lines (Fig. 1) represent the relation to transfer the AMSR-E sensor calibration into the future by means of TMI and are applied for intercalibration purposes to the AMSR2 sensor. An example of such intercalibration is given for the X-band frequency at horizontal polarization (top left); however, this principle holds for all frequencies and polarizations. The first set of regression parameters allows expressing brightness temperature observations of the AMSR-E sensor as a function of brightness temperatures observed by the TMI sensor [Eq. (1)]. Therefore, these regressions have the capacity to act as a memory of the sensor calibration of AMSR-E observations through time. The second set of regressions actually applies this transferred sensor calibration of AMSR-E (by means of TMI) to observations of AMSR2 [Eq. (2)]. The aim of this procedure is to align the observations from the AMSR2 sensor with those of the AMSR-E sensor in which TMI only acts as a platform to transfer the sensor calibration through time:

$$T_{b_{\mathrm{AMSR\text{-}E10.7}(H)}} = 0.98 T_{b_{\mathrm{TMI10.65}(H)}} + 8.81 \qquad (1)$$

and

$$T_{b_{\mathrm{AMSR210.7}(H)}} = 1.02 T_{b_{\mathrm{TMI10.65}(H)}} - 5.28. \qquad (2)$$

It is assumed that small differences in sensor specifications (Table 1) between TMI and both AMSR sensors are not relevant in this intercalibration procedure, since the latter have the same specifications. The result of the slightly different specifications between TMI and both AMSR sensors will provide similar consistency with TMI brightness temperatures. Therefore, the interaction between both AMSR sensors and the slightly divergent TMI sensor is assumed to be identical for the AMSR-E–TMI and the AMSR2–TMI sensor combinations.

c. *Radio frequency interference*

The natural microwave emission of the surface is very low in energy and can easily be masked by man-made sources, which can ultimately have a significant impact on soil moisture products. RFI can be caused by instruments such as radars, wireless communications, and satellite television broadcasts, and disturbed observations are usually masked from further analysis (e.g., de Jeu et al. 2008; Oliva et al. 2012). The almost decadal AMSR-E dataset revealed systematic RFI problems in the lowest C-band (6.9 GHz) frequency over the United States, the Middle East, India, and Japan (e.g., Li et al. 2004; Parinussa et al. 2011a). To avoid RFI-related problems in these regions, a neighboring channel in a closely related frequency but without overlapping bandwidths (7.3 GHz; see Table 1) was added to AMSR2.

As an indication for RFI in AMSR2, we adapted the detection algorithm developed by Li et al. (2004). The observations in the neighboring C-band frequency (7.3 GHz) were linearly matched to those of the lowest C-band frequency (6.9 GHz) at the global scale in order to adopt the thresholds from Li et al. (2004). Figure 2 (top) indicates a diagnostic for RFI in the 6.9-GHz channel, showing the previously mentioned regions notorious for RFI. Though it does not impact the purpose of this study, it should be noted that Greenland appears to be contaminated. Snow-covered regions are known for unusual background emission (Seto et al. 2005), which likely results in RFI flagging and confirms the hypothesis that RFI flagging most likely occurs because of unusual background emission of snow-covered regions. A completely new view on this topic is shown in Fig. 2 (middle), presenting a diagnostic for RFI contamination in the neighboring C-band frequency (7.3 GHz). Many new regions appear to be contaminated, such as Morocco, Turkey, eastern Europe, western Russia, Bangladesh, Cambodia, Vietnam, and Indonesia. On the other hand, the addition of this neighboring channel was developed with the goal to serve as a replacement in regions with known contamination in the lowest C-band channel (6.9 GHz), mainly Japan and the continental United States. Figure 2 (bottom) shows the success of this approach, providing almost RFI-free coverage of C-band observations globally. More in-depth research is needed to provide a more comprehensive view on this topic. In any case, the results demonstrate the delicacy of RFI in passive microwave observations and clearly show the need for observations in a range of frequencies in order to derive an uncontaminated global picture.

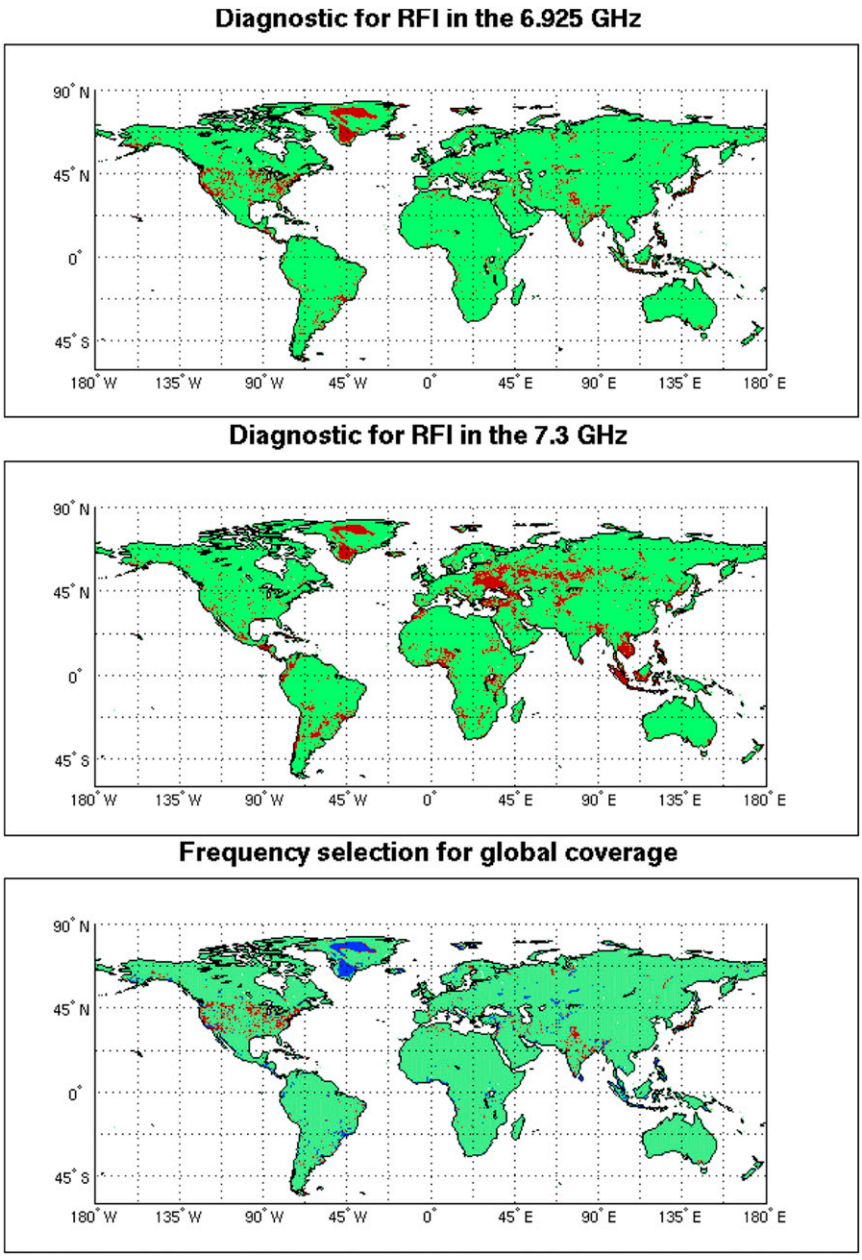

FIG. 2. RFI maps for the (top) lowest-frequency channel (6.9 GHz) and (middle) neighboring frequency channel (7.3 GHz). (bottom) A selection map to reach global coverage of uncontaminated AMSR2 observations. Green represents the use of the lowest channel, red represents the use of the neighboring C-band channel, and blue represents the use of the X-band frequency channel.

3. Land surface parameters

a. The Land Parameter Retrieval Model

AMSR-E was one of the first sensors widely used for the retrieval of global surface soil moisture, and a number of retrieval algorithms have been developed (e.g., Njoku et al. 2003; Jackson et al. 2004; Owe et al. 2008; Jones et al. 2010). One of these retrieval algorithms is the Land Parameter Retrieval Model (LPRM; Owe et al. 2008) that was also applied to various other passive microwave sensors. LPRM is one of the more comprehensive models, as it simultaneously retrieves soil moisture, vegetation optical depth, and the uncertainty of the retrieved soil moisture value (Parinussa et al. 2011b). LPRM is based on a simple radiative transfer equation and uses the analytical derivation of Meesters

et al. (2005) to partition the microwave observation (polarized C or X band) into its respective soil and vegetation components. The LPRM uses an external algorithm for land surface temperature; Holmes et al. (2009) proposed a linear relationship between vertically polarized Ka-band observations to obtain land surface temperature. LPRM was detailed in a range of publications (e.g., Owe et al. 2008; Parinussa et al. 2012; de Jeu et al. 2014) to which readers are directed for more information on this retrieval algorithm.

LPRM soil moisture products have been extensively validated against in situ observations (e.g., Wagner et al. 2007; Draper et al. 2009; Brocca et al. 2011; Parinussa et al. 2012), models (e.g., Bisselink et al. 2011; Rebel et al. 2012; Wanders et al. 2012), and other satellite products (e.g., Scipal et al. 2008; Dorigo et al. 2010; Crow et al. 2010). These studies indicate the high skill of LPRM in capturing the temporal variability in observed soil moisture. Moreover, a multidecadal (30+ years) soil moisture product was already developed within ESA's CCI program with a prominent role for this retrieval algorithm. These two key arguments motivate the use of LPRM in this study.

b. *Reanalysis soil moisture data*

ERA-Interim is a global atmospheric reanalysis product developed by the European Centre for Medium-Range Weather Forecasts (ECMWF), covering the period from 1 January 1979 onward, and is also available in near–real time (Dee et al. 2011). Gridded data of a large variety of surface parameters are available at a 3- and/or 6-hourly temporal resolution at a spatial resolution of approximately 0.70°. Daily average soil moisture from the shallowest (0–7 cm) soil layer of the ERA-Interim product was gridded into 0.25° × 0.25° regular grids using the nearest neighbor resampling technique. Remotely sensed and reanalysis products share well-known similarities and differences (e.g., Albergel et al. 2010; Taylor et al. 2012; Dorigo et al. 2015) as a result of the observational nature of the former versus the modeled nature of the latter. The goal of this study is not to analyze (non)shared behavior between remotely sensed and reanalysis surface soil moisture, but ERA-Interim serves as a consistent reference product covering the nonoverlapping periods of AMSR-E and AMSR2.

c. *In situ soil moisture observations*

The International Soil Moisture Network (ISMN) is an online, freely accessible database of in situ soil moisture observations and is hosted by the Vienna University of Technology (Dorigo et al. 2011, 2013; http://ismn.geo.tuwien.ac.at/). This database is intended to serve for the validation of remotely sensed soil moisture products as well as land surface models. Based on the recentness of the satellite products used, four ground-based networks were selected from the ISMN: Soil Climate Analysis Network (SCAN; United States), Red de Medición de la Humedad del Suelo (REMEDHUS; Spain), Terrestrial Environmental Observatories (TERENO; Germany), and Umbria (Italy), which all contain multiple sensors within a single satellite footprint. First, the performance of the AMSR-E and AMSR2 sensors against in situ soil moisture time series that cover both individual periods is examined, which allows for evaluation of the consistency between these nonoverlapping periods. Next, the performance compared to the ground-based observations themselves and the performance relative to two currently operational remotely sensed soil moisture products (section 3d) are assessed. These aims motivate the use of all available sensors over these networks without a priori selection. Only two criteria were used in order to determine whether observations from a specific sensor in these networks are used in this analysis. The first is a total observation period of at least 3 months within the entire period that was analyzed (from July 2012 to August 2013 for AMSR2), a criteria that all remotely sensed soil moisture products need to pass in order to include them for further analysis. A simple test for representativeness of the ground-based observations at satellite scale also needs to be passed. The second is that the ERA-Interim soil moisture products require a positive correlation with the ground-based observations, as in Dorigo et al. (2015). These criteria eventually resulted in 21 stations over the REMEDHUS network, 89 stations over the SCAN network, 18 stations over the TERENO network, and 7 stations over the Umbria network.

d. *Other remotely sensed soil moisture products*

The Advanced Scatterometer (ASCAT) is a radar instrument on board the MetOp meteorological satellites operated by the European Organisation for the Exploitation of Meteorological Satellites (EUMETSAT) in collaboration with ESA. ASCAT operates in the C-band (5.255 GHz) frequency and operates on the *MetOp-A* platform, which started its operation in October 2006. The Vienna University of Technology soil moisture change detection algorithm (Naeimi et al. 2009) uses backscatter measurements at six different azimuth angles to calculate soil moisture. The retrieved value is a relative measure of surface (1–2 cm) soil moisture ranging between wilting point and saturation.

The SMOS satellite (Kerr et al. 2010) is the first dedicated satellite mission to observe soil moisture. This satellite was launched in November 2009 and observes Earth's surface at multiple incidence angles in the L-band (1.4 GHz) frequency. The multi-incidence

retrieval algorithm L-band Microwave Emission of the Biosphere (L-MEB) was developed in order to retrieve surface (1–5 cm) soil moisture. In this study, we used the SMOS soil moisture product version 600, which is the most recent dataset at the time of writing. Observations from SMOS are hampered by RFI contamination, especially over Europe (Oliva et al. 2012). Potentially contaminated soil moisture retrievals have been removed using the appropriate flags, as well as soil moisture retrievals exceeding an uncertainty of $0.04\,m^3\,m^{-3}$.

4. A comparison of the soil moisture products

a. *ERA-Interim*

The impact of the intercalibration scenarios on the soil moisture retrievals from AMSR-E and AMSR2 was first tested. The LPRM was applied to AMSR-E and AMSR2 observations for their respective nonoverlapping periods for each of these scenarios. Soil moisture retrievals from these were compared to the ERA-Interim reference dataset that is consistently modeled for these two nonoverlapping periods. The analysis periods for both sensors were chosen to be equally long: for AMSR-E this was from December 2010 to October 2011, while for AMSR2 this period was from July 2012 to May 2013. The bias (left) and root-mean-square error (RMSE; right) were evaluated at the global scale and results were presented in Fig. 3. Each density plot shows these statistics for the AMSR-E and ERA-Interim soil moisture product on the x axis and the same statistics for the AMSR2 and ERA-Interim soil moisture product on the y axis for each of the scenarios. As we mentioned earlier, the soil moisture products that were compared share well-known similarities and differences (e.g., Albergel et al. 2010; Taylor et al. 2012; Dorigo et al. 2015). Additionally, ERA-Interim data come in a different spatial and temporal frequency and the vertical support is 0–7 cm, whereas the remotely sensed products represent a much shallower layer. It should also be mentioned that the goal of this exercise is not to analyze (non)shared behavior between remotely sensed and reanalysis surface soil moisture, but ERA-Interim serves as a consistent reference product covering the nonoverlapping periods of AMSR-E and AMSR2. Therefore the explicit rationale behind this evaluation is that a closer match to the 1:1 line lends more confidence in the scenario that was applied for intercalibration.

The first three rows of Fig. 3 present the scenarios in which no intercalibration procedure was applied in order to line up AMSR2 brightness temperature observations with those of AMSR-E. The soil moisture retrievals from the lowest frequency (6.9 GHz) show a very close match to the 1:1 line, with a slope of 0.986 and an offset of −0.007 for the bias and a slope of 0.963 and an offset of 0.012 for the RMSE. It is repeated that both bias and RMSE contain error sources from both the remotely sensed as well as the modeled soil moisture data. The second row presents the soil moisture retrievals from the lowest-frequency (6.9 GHz) channel of AMSR-E against the soil moisture retrievals from AMSR2 from the neighboring channel (7.3 GHz) of AMSR2. Theoretically, they should slightly differ because of the 0.4 GHz difference in center frequency. In contrast with the previously discussed lowest-frequency (6.9 GHz) channels, this comparison shows a clear deviation between the linear regressions (dashed line) from the 1:1 line (solid line). This deviation is considerably larger than can be expected from only the 0.4-GHz difference in center frequency. For soil moisture retrievals from the X-band (10.7 GHz) channel (third row), this deviation from the 1:1 line is even larger, which clearly demonstrates the urgent need for an additional intercalibration step.

The fourth and fifth rows present the global results obtained for the soil moisture retrievals from the X-band channel (10.7 GHz) after the application of the results of the intercalibration procedure. The fourth row shows these relations after the application of the strictest filtering steps based on frozen conditions, snowy conditions, heterogeneous land cover, open water fraction, active precipitation, and sample sizes (section 2b). A significant improvement compared to the scenario that was not intercalibrated (third row) was evident after implementing the results of this strictest filtering scenario. The fifth row shows the scenario in which we used all terrestrial brightness temperature observations for intercalibration purposes and shows an even closer match to the 1:1 line. The bias shows a slope value of 0.978 and an offset of 0.008, whereas the RMSE shows a slope value of 0.955 and an offset of 0.022. For this reason, this scenario that uses all terrestrial brightness temperatures for intercalibration purposes is considered to be best suited to reach the goal of this particular study.

Figure 4 presents the spatial distribution of the coefficient of determination R^2 ($P < 0.05$) between ERA-Interim and both AMSR-E (Fig. 4a) and AMSR2 (Fig. 4b) soil moisture products retrieved from X-band observations at the global scale. Again, we should emphasize that modeled and remotely sensed soil moisture products share well-known similarities and differences (e.g., Albergel et al. 2010; Taylor et al. 2012; Dorigo et al. 2015) and that this frequency band is not optimal for soil moisture retrievals (e.g., Parinussa et al. 2011b). We should also note that the fraction of open water and the land surface temperature bias threshold (section 2b) were used for masking its respective soil moisture data.

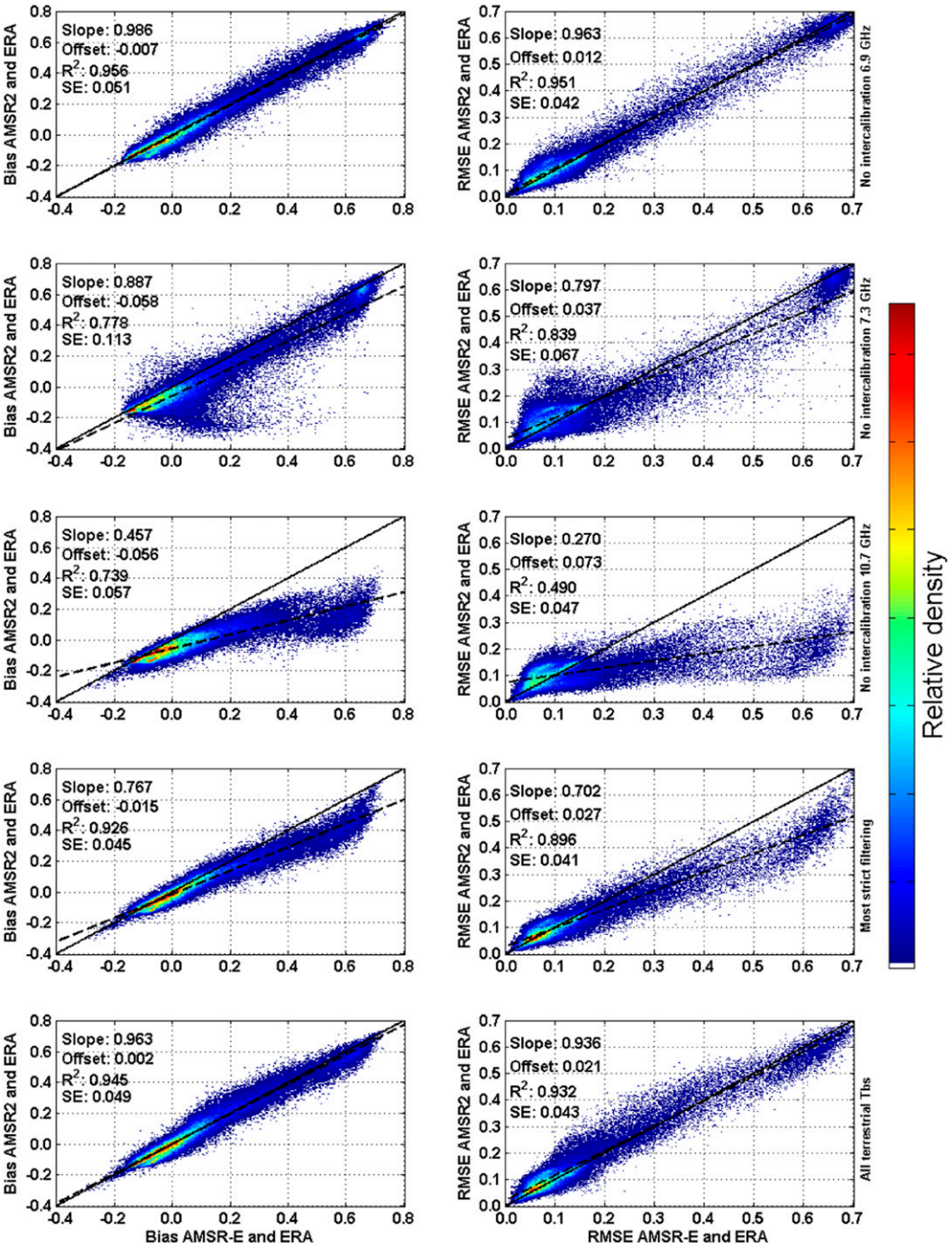

FIG. 3. Global comparison between the remotely sensed soil moisture products from AMSR-E and AMSR2 as compared to the fixed ERA-Interim dataset ($m^3 m^{-3}$). Three different intercalibration scenarios were tested and the global-scale impact on the (left) bias and (right) RMSE was shown. The linear regression was represented by the dashed lines and the 1:1 line was represented by the solid lines.

A distinct spatial pattern was observed in the comparison between soil moisture from the reanalysis and remote sensing, with high values of R^2 in semiarid climate regimes and low agreement in the tropical rain forests and boreal regions. As previously mentioned, the aim of this study is not to analyze (non)shared behavior between reanalysis and remotely sensed products but to show consistency between the soil moisture products retrieved from AMSR-E and AMSR2 in their nonoverlapping periods. The high spatial correlation coefficient

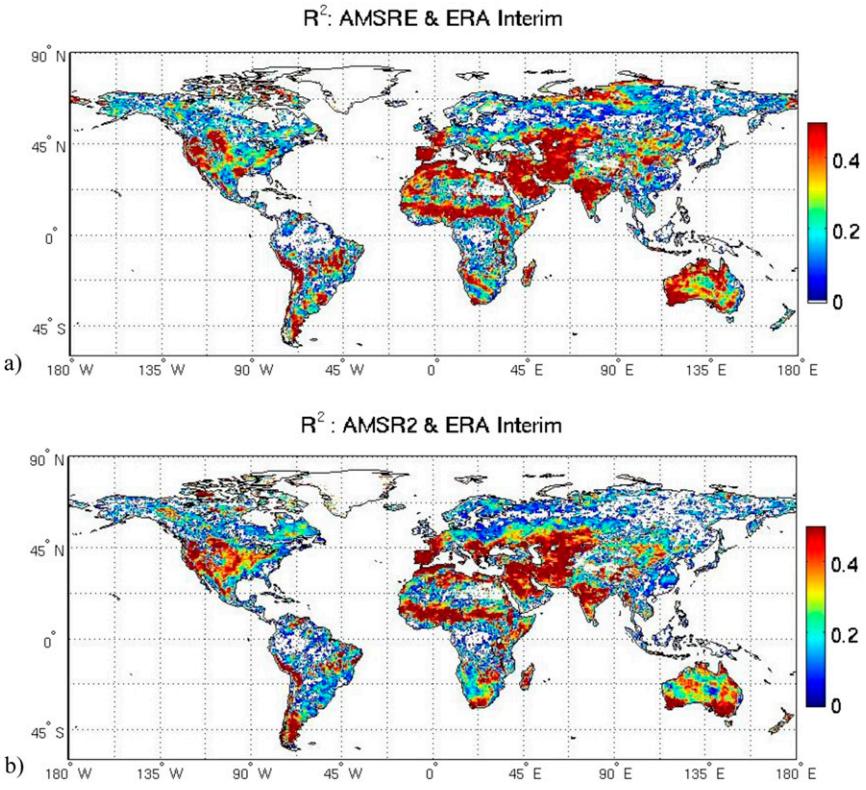

FIG. 4. Global maps of R^2 ($P < 0.05$) between the AMSR-E and ERA-Interim and the AMSR2 and ERA-Interim combinations. A distinct spatial pattern was observed in the comparison between soil moisture from the reanalysis and remote sensing with high values of R^2 in semiarid climate regimes.

($R = 0.64$) of both R^2 maps shows consistency between the remotely sensed soil moisture products retrieved from the AMSR-E and AMSR2 sensors.

b. *Ground-based observations*

To further investigate the consistency of the soil moisture retrieved from observations of the AMSR-E and AMSR2 sensors, we also performed analysis against ground-based observations from the four different in situ soil moisture networks. The rationale behind this analysis is similar to the comparison against ERA-Interim soil moisture, meaning that a closer match to the 1:1 line lends more confidence in the consistency between AMSR-E and AMSR2. The statistics (bias and RMSE) between the in situ and remotely sensed soil moisture product from AMSR-E were plotted on the x axis whereas these statistics against AMSR2 were plotted at the y axis. The results were presented in Fig. 5, separated for bias values (top) and RMSE (bottom). The crosses represent the statistical values of the comparison between the remotely sensed and ground-based soil moisture products from either AMSR-E (x axis) or AMSR2 (y axis). The colors indicate whether the soil moisture was retrieved from the X-band observations (blue) or from the C-band observations (red). Here, it is also emphasized that obtained results should be interpreted with care. Remotely sensed and in situ soil moisture also share well-known differences, such as their observation depth and spatial representation and the destructive nature of the latter. The relatively close match between both regression lines is an indicator for consistency between the remotely sensed soil moisture products in these nonoverlapping time frames.

Several other remotely sensed global soil moisture products, such as the ASCAT and SMOS products, are also available. Additional comparisons of these products, as well as the newly developed AMSR2 soil moisture product, against ground-based observations from the ISMN (section 3c) were also performed. Table 2 presents the mean correlation coefficient and RMSE for each of these remotely sensed soil moisture products against in situ data. As the remotely sensed products operate in unique frequencies, they also have their unique characteristics (e.g., sensing depth); additionally, the remotely sensed products come in different units ($m^3\,m^{-3}$ for SMOS and LPRM or degree of saturation

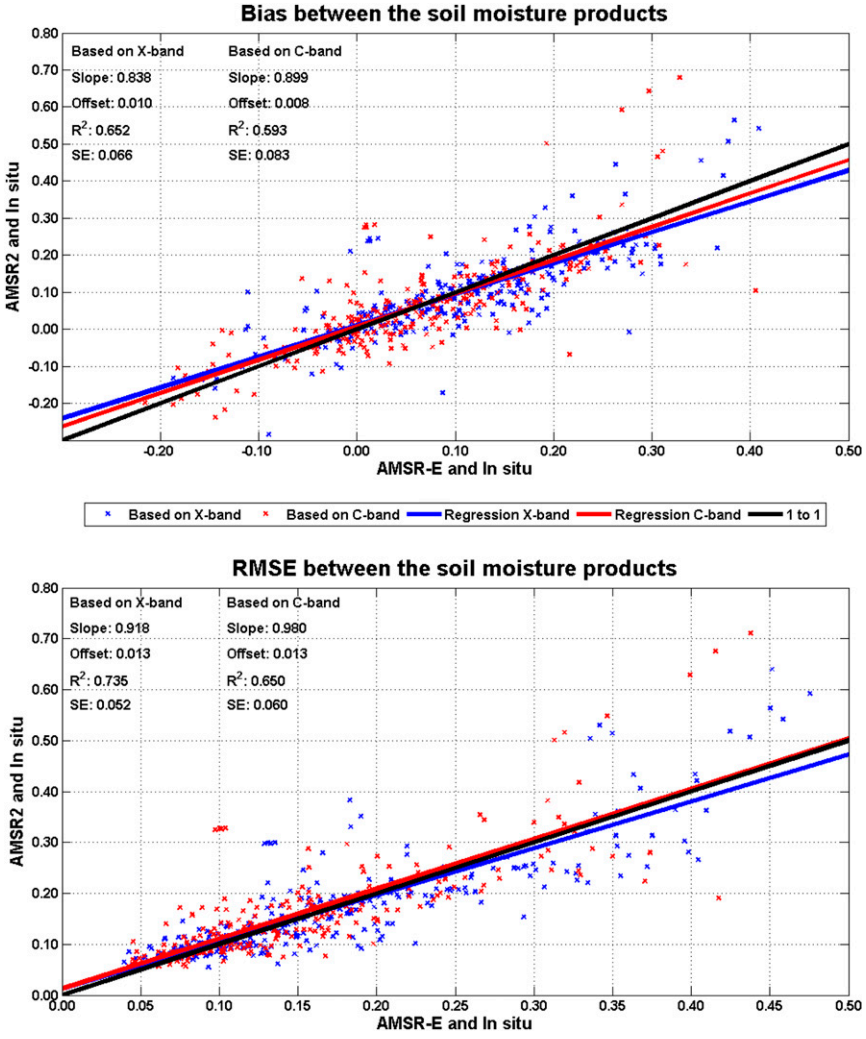

FIG. 5. The consistency of the AMSR-E and AMSR2 soil moisture products as retrieved from the X-band (blue) and lowest C-band (red) frequencies evaluated against in situ soil moisture from the ISMN using (top) bias and (bottom) RMSE. The crosses represent the individual ground stations, and the solid lines represent their linear regressions and the 1:1 line (solid line).

for ASCAT). Therefore, we normalized each remotely sensed product to match the mean and standard deviation of the ground-based observations before calculating the RMSE (Table 2). Daytime and nighttime observations were explicitly separated, as these are known to vary as a result of different physics (e.g., de Jeu et al. 2008; Parinussa et al. 2011a). The newly derived AMSR2 soil moisture product shows a very high performance (R = 0.79 for nighttime and R = 0.82 for daytime observations) over the REMEDHUS network. The ASCAT soil moisture product shows a performance of equal level. However, SMOS shows a somewhat lower performance at the in situ networks. The SMOS and AMSR2 product have a similar performance over the SCAN sites in the United States, whereas the performance of ASCAT somewhat drops. These averaged results should be interpreted as first guess numbers, and more thorough verification studies are expected to provide a more comprehensive view regarding this topic.

The lower performance of SMOS over Europe may be explained by the unexpected RFI contamination encountered in the protected L-band frequency over this continent (Oliva et al. 2012). The correlation values of AMSR2 over the semiarid REMEDHUS network are in line with theory and the results obtained for its predecessor (e.g., Dorigo et al. 2010; Brocca et al. 2011; Wanders et al. 2012). The lower performance of the AMSR2 soil moisture product over the TERENO network is also in line with theory, as this network is located in a more forested region and is therefore not beneficial for soil moisture retrievals from the LPRM (Parinussa et al. 2011b). In any case, these averaged results serve as

TABLE 2. Averaged correlation coefficients and RMSE for the remotely sensed soil moisture products compared to ground-based observations over the four different soil moisture networks. Daytime and nighttime observations were explicitly separated.

		AMSR2		SMOS		ASCAT	
Observations	ISMN network (stations)	*R*	RMSE	*R*	RMSE	*R*	RMSE
Nighttime	REMEDHUS (21)	0.79	0.04	0.69	0.05	0.83	0.04
	SCAN (89)	0.41	0.06	0.39	0.07	0.29	0.07
	Tereno (18)	0.64	0.05	0.34	0.07	0.67	0.05
	Umbria (7)	0.78	0.06	0.35	0.12	0.84	0.06
Daytime	REMEDHUS (21)	0.82	0.04	0.65	0.05	0.76	0.05
	SCAN (89)	0.38	0.07	0.39	0.06	0.37	0.07
	Tereno (18)	0.49	0.06	0.43	0.07	0.63	0.06
	Umbria (7)	0.68	0.08	0.46	0.09	0.82	0.06

rough indications but actually show variation of the performance of all remotely sensed soil moisture products.

c. *Soil moisture and precipitation data over the Australian continent*

Systematic differences between the AMSR-E and AMSR2 soil moisture products may exist as a result of inconsistencies in the radiometer intercalibration procedure. Data users should always be aware of systematic differences, particularly when analyzing the combination of the AMSR-E and AMSR2 sensors. In a first attempt to analyze a combination of LPRM soil moisture products from these two sensors, a case study for Australia using the soil moisture products retrieved from X-band observations is presented. The intention of this case study is to show that soil moisture climatology from AMSR-E observations can effectively be used to calculate soil moisture anomalies from AMSR2 observations.

The Australian continent was selected for its monotonic climate regime and sparse vegetation cover, which makes it extremely suitable for microwave remote sensing of soil moisture. Additionally, unusual variations over the Australian continental climate are observed from September 2012 onward (Bureau of Meteorology 2013), which is a period coinciding with the AMSR2 observation period. The long-term (2007–11) soil moisture climatology of AMSR-E was combined with soil moisture retrievals from AMSR2 in order to determine soil moisture anomalies (2012–13). Decomposition in an anomaly and climatology component is common practice in climate studies and data assimilation (Reichle and Koster 2004; Crow et al. 2010) to minimize systematic differences. To determine the potential for combining soil moisture observations of the AMSR-E and AMSR2 sensor, we (visually) compared these soil moisture anomalies to precipitation percentages presented by the Australian Bureau of Meteorology (Fig. 6). Although soil moisture saturation problems could occur under wet conditions, the obvious physical relationship between precipitation and surface soil moisture enables a comparison between these two anomaly maps.

A distinct gradient in both precipitation and surface soil moisture was observed in September 2012 over the entire Australian continent. The state of Western Australia was generally wetter than expected, with the exception of its western tip (Shark Bay extending to Geraldton) and its southeastern corner extending toward the Cook region. These dry regions, together with the wetter region in the northern part of this state, are profound in both the precipitation and soil moisture datasets. The central and eastern part of the Australian continent generally show drier conditions than expected based on the climatological values; these patterns are also profound in both datasets. Another feature in both images is the north-to-south gradient in the eastern part of the Australian continent with a decreasing water shortage extending southward into Victoria. The far eastern part of the Australian continent was masked (gray) from the comparison because this region contains dense vegetation, which is a reason for degrading quality of soil moisture products (e.g., Dorigo et al. 2010; Parinussa et al. 2011b). Although the comparison between remotely sensed soil moisture and precipitation datasets is only visual, similarities in both maps lend confidence to the newly developed soil moisture anomaly product that uses the AMSR-E climatology. Soil moisture and precipitation are related variables, but they are also fundamentally different components of the hydrological system. The agreement in their spatial patterns; distinction of wet and dry regions (positive or negative anomalies); and, to a somewhat lesser extent, their relative magnitudes suggest potentially high synergy between the AMSR-E and AMSR2 soil moisture products as retrieved from X-band observations.

5. Conclusions and outlook

This preliminary study presents a potential approach toward synergy between soil moisture products retrieved from AMSR-E and AMSR2 X-band observations. The

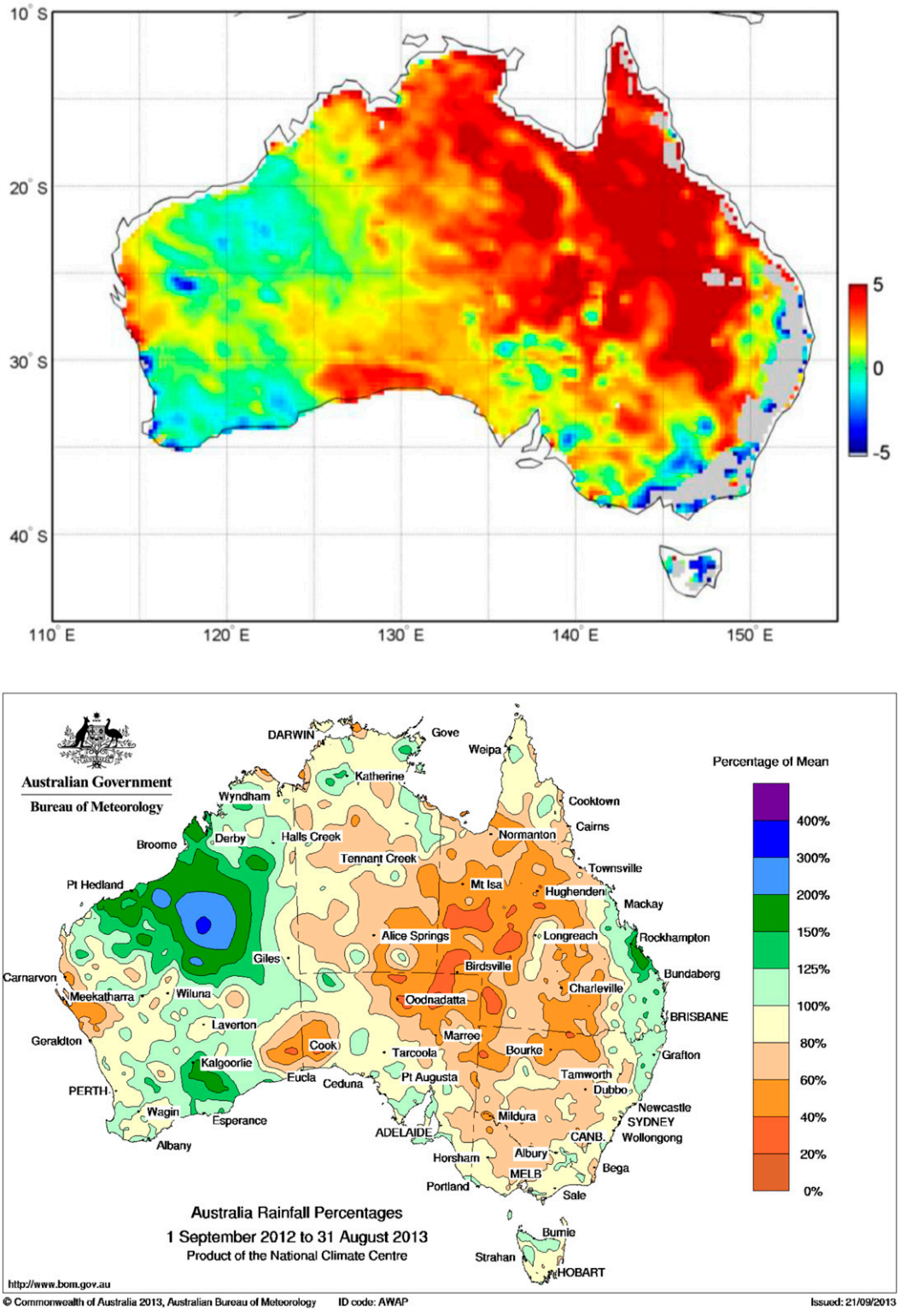

FIG. 6. A visual comparison over the Australian continent between soil moisture anomalies based on (top) a combination of AMSR-E and AMSR2 and (bottom) precipitation percentages of the long-term climatology as presented by the Australian Bureau of Meteorology (www.bom.gov.au). Image courtesy of the Commonwealth of Australia (ID code AWAP; issued on 21 Sep 2013).

TMI sensor transfers the calibration of the AMSR-E sensor into the future in an attempt to reach consistency with the AMSR2 sensor. Novel surface soil moisture retrievals from both AMSR2 C-band frequency channels were also presented and compared against the two independent reference soil moisture datasets (reanalysis and in situ soil moisture). An extension of the available WindSat dataset, which is currently only a single month between the WindSat and AMSR2 sensors, will likely lead to improved consistency between soil moisture products retrieved from the C-band frequency channels.

A global comparison of soil moisture retrievals against ERA-Interim soil moisture demonstrates the absolute need for an intercalibration procedure, particularly for the X-band channel (10.7 GHz) and, to a smaller extent, the neighboring C-band channel (7.3 GHz). After the implementation of such a procedure using the TMI as a transition platform, a high spatial correlation coefficient ($R = 0.64$) of both R^2 maps shows consistency between the remotely sensed soil moisture products retrieved from the AMSR-E and AMSR2 sensors. A comparison of the newly derived AMSR2 product to ground-based observations shows results in line with the heritage left by AMSR-E. Additional comparison over the ground networks revealed that AMSR2 soil moisture products are complementary to two existing remotely sensed soil moisture products. It was also shown that RFI in both C-band (6.9 and 7.3 GHz) channels is of considerable importance. The neighboring C-band frequency (7.3 GHz) clearly showed its potential to serve as a replacement over the regions notorious for RFI contamination (e.g., United States, the Middle East, India, and Japan) in the lowest C-band frequency (6.9 GHz). More extensive RFI detection algorithms need to be developed in the future in order to get a better handle on this topic, with special emphasis on natural background radiation. With this example, we show that there is a need for multifrequency observations when aiming for global coverage of the soil moisture retrievals. Additionally, a case study over the Australian continent shows high spatial agreement between a long-term precipitation dataset and soil moisture anomalies as derived from a combination of the AMSR-E and AMSR2 sensors. The exact level of synergy between these two sensors, particularly for global-scale (trend) studies, remains a topic for future research. As the LPRM AMSR2 dataset is progressing over time, it is expected that its own observation record may also be used to reliably decompose the dataset into its respective soil moisture climatology and anomaly components in the future.

The newly derived products of the LPRM AMSR2 combination are available for user download via the Goddard Earth Sciences Data and Information Services Center (GES DISC). In accordance with past and current data streams, these data are expected to become available within a few hours of the arrival of the input AMSR2 data at the GES DISC. The actual data latency of LPRM AMSR2 will depend on the availability of the AMSR2 data. The results presented in this preliminary study can serve as a starting point for potential users of this LPRM AMSR2 data stream. Extensive user feedback, as the developers of these products have regularly received in the past, is expected to help improve the retrieval algorithm and intercalibration procedure and thus improve the consistency between geophysical retrievals from the AMSR-E and AMSR2 sensors in the future. Care should be taken in the interpretation of the products from both AMSR-E and the newly developed AMSR2 sensors, as these products may suffer systematic differences. Finally, the results clearly show the need for an intercalibration procedure in order to minimize such systematic differences.

Acknowledgments. This work has been undertaken as part of the European Space Agency Climate Change Initiative for soil moisture (www.esa-soilmoisture-cci.org), Contract 4000104814/11/I-NB. Additionally, this work was funded by the European Commission's 7th Framework project, under Grant Agreement 282672, EMBRACE project. Niko Wanders was funded by a grant from the user support program Space Research of NWO (Contract NWO GO-AO/30). The authors greatly thank William Teng and Fan Fang from the GES DISC, as part of a NASA-funded project NNH08ZDA001N-DECISIONS, for providing the WindSat data. The authors also like to thank the European Centre for Medium-Range Weather Forecasts for making the verification data available.

REFERENCES

Albergel, C., and Coauthors, 2010: Cross-evaluation of modelled and remotely sensed surface soil moisture with in situ data in southwestern France. *Hydrol. Earth Syst. Sci.,* **14,** 2177–2191, doi:10.5194/hess-14-2177-2010.

Beck, H. E., R. A. M. de Jeu, J. Schellekens, A. I. J. M. van Dijk, and L. A. Bruijnzeel, 2009: Improving curve number based storm runoff estimates using soil moisture proxies. *IEEE J. Sel. Topics Appl. Earth Observ.,* **2,** 250–259, doi:10.1109/JSTARS.2009.2031227.

Bisselink, B., E. van Meijgaard, A. J. Dolman, and R. A. M. de Jeu, 2011: Initializing a regional climate model with satellite-derived soil moisture. *J. Geophys. Res.,* **116,** D02121, doi:10.1029/2010JD014534.

Brocca, L., F. Melone, T. Moramarco, W. Wagner, V. Naeimi, Z. Bartalis, and S. Hasenauer, 2010: Improving runoff prediction through the assimilation of the ASCAT soil moisture product. *Hydrol. Earth Syst. Sci.,* **14,** 1881–1893, doi:10.5194/hess-14-1881-2010.

——, and Coauthors, 2011: Soil moisture estimation through ASCAT and AMSR-E sensors: An intercomparison and validation study across Europe. *Remote Sens. Environ.,* **115,** 3390–3408, doi:10.1016/j.rse.2011.08.003.

——, F. Ponziani, T. Moramarco, F. Melone, N. Berni, and W. Wagner, 2012: Improving landslide forecasting using ASCAT-derived soil moisture data: A case study of the Torgiovannetto landslide in central Italy. *Remote Sens.,* **4,** 1232–1244, doi:10.3390/rs4051232.

Bureau of Meteorology, 2013: Special climate statement 46—Australia's warmest September on record. Bureau of Meteorology, Australian Government, 26 pp. [Available online at www.bom.gov.au/climate/current/statements/scs46.pdf.]

Cook, R. D., 1977: Detection of influential observations in linear regression. *Technometrics,* **19** (1), 15–18.

Crow, W. T., D. G. Miralles, and M. H. Cosh, 2010: A quasi-global evaluation system for satellite based surface soil moisture retrievals. *IEEE Trans. Geosci. Remote Sens.,* **48,** 2516–2527, doi:10.1109/TGRS.2010.2040481.

Dee, D. P., and Coauthors, 2011: The ERA-Interim reanalysis: Configuration and performance of the data assimilation system. *Quart. J. Roy. Meteor. Soc.,* **137,** 553–597, doi:10.1002/qj.828.

de Jeu, R. A. M., W. Wagner, T. R. H. Holmes, A. J. Dolman, N. van de Giesen, and J. Friesen, 2008: Global soil moisture patterns observed by space borne microwave radiometers and scatterometers. *Surv. Geophys.,* **29,** 399–420, doi:10.1007/s10712-008-9044-0.

——, T. R. H. Holmes, R. M. Parinussa, and M. Owe, 2014: A spatially coherent global soil moisture product with improved temporal resolution. *J. Hydrol.,* **516,** 284–296, doi:10.1016/j.jhydrol.2014.02.015.

Dorigo, W. A., K. Scipal, R. M. Parinussa, Y. Y. Liu, W. Wagner, R. A. M. de Jeu, and V. Naeimi, 2010: Error characterization of global active and passive microwave soil moisture datasets. *Hydrol. Earth Syst. Sci.,* **14,** 2605–2616, doi:10.5194/hess-14-2605-2010.

——, P. van Oevelen, W. Wagner, M. Drusch, S. Mecklenburg, A. Robock, and T. Jackson, 2011: A new international network for in situ soil moisture data. *Eos, Trans. Amer. Geophys. Union,* **92,** 141–142, doi:10.1029/2011EO170001.

——, A. Xaver, M. Vreugdenhil, A. Gruber, A. Hegyiova, A. D. Sanchis-Dufau, W. Wagner, and A. Drusch, 2013: Global automated quality control of in-situ soil moisture data from the International Soil Moisture Network. *Vadose Zone J.,* **12,** doi:10.2136/vzj2012.0097.

——, and Coauthors, 2015: Evaluation of the ESA CCI soil moisture product using ground-based observations. *Remote Sens. Environ.,* doi:10.1016/j.rse.2014.07.023, in press.

Draper, C., J. Walker, P. Steinle, R. A. M. de Jeu, and T. R. H. Holmes, 2009: An evaluation of AMSR-E derived soil moisture over Australia. *Remote Sens. Environ.,* **113,** 703–710, doi:10.1016/j.rse.2008.11.011.

Entekhabi, D., and Coauthors, 2010: The Soil Moisture Active and Passive (SMAP) mission. *IEEE Proc.,* **98,** 704–716, doi:10.1109/JPROC.2010.2043918.

Gaiser, P., and Coauthors, 2004: The WindSat Spaceborne Polarimetric Microwave Radiometer: Sensor description and early orbit performance. *IEEE Trans. Geosci. Remote Sens.,* **42,** 2347–2360, doi:10.1109/TGRS.2004.836867.

GCOS, 2010: Implementation plan for the global observing system for climate in support of the UNFCCC. WMO/TD 1244, 23 pp. [Available online at https://www.wmo.int/pages/prog/gcos/Publications/gcos-92_GIP_ES.pdf.]

Hollmann, R., and Coauthors, 2013: The ESA Climate Change Initiative: Satellite data records for essential climate variables. *Bull. Amer. Meteor. Soc.,* **94,** 1541–1552, doi:10.1175/BAMS-D-11-00254.1.

Holmes, T. R. H., R. A. M. De Jeu, M. Owe, and A. J. Dolman 2009: Land surface temperature from Ka band (37 GHz) passive microwave observations. *J. Geophys. Res.,* **114,** D04113, doi:10.1029/2008JD010257.

——, W. T. Crow, M. Tugrul Yilmaz, T. J. Jackson, and J. B. Basara, 2013: Enhancing model-based land surface temperature estimates using multiplatform microwave observations. *J. Geophys. Res. Atmos.,* **118,** 577–591, doi:10.1002/jgrd.50113.

Imaoka, K., M. Kachi, M. Kasahara, N. Ito, K. Nakagawa, and T. Oki, 2010: Instrument performance and calibration of AMSR-E and AMSR2. *Int. Arch. Photogramm., Remote Sens. Spat. Inf. Sci.,* **38** (8), 13–16. [Available online at www.isprs.org/proceedings/XXXVIII/part8/pdf/JTS13_20100322190615.pdf.]

Jackson, T., R. Hurkmans, A. Hsu, and M. Cosh, 2004: Soil moisture algorithm validation using data from the Advanced Microwave Scanning Radiometer (AMSR-E) in Mongolia. *Riv. Ital. Telerilevamento,* **30,** 37–50.

Jones, L. A., C. R. Ferguson, J. S. Kimball, K. Zhang, S. K. Chan, K. C. McDonald, E. G. Njoku, and E. F. Wood, 2010: Daily land surface air temperature retrieval from AMSR-E: Comparison with AIRS/AMSU. *IEEE J. Appl. Earth Obs. Remote Sens.,* **3,** 111–123, doi:10.1109/JSTARS.2010.2041530.

Jung, M., and Coauthors, 2010: Recent decline in the global land evapotranspiration trend due to limited moisture supply. *Nature,* **467,** 951–954, doi:10.1038/nature09396.

Kerr, Y., and Coauthors, 2010: The SMOS mission: New tool for monitoring key elements of the global water cycle. *IEEE Proc.,* **98,** 666–687, doi:10.1109/JPROC.2010.2043032.

Kummerow, C., W. Barnes, T. Kozu, J. Shiue, and J. Simpson, 1998: The Tropical Rainfall Measuring Mission (TRMM) sensor package. *J. Atmos. Oceanic Technol.,* **15,** 809–817, doi:10.1175/1520-0426(1998)015<0809:TTRMMT>2.0.CO;2.

Li, L., E. Njoku, E. Im, P. Chang, and K. Germaine, 2004: A preliminary survey of radio frequency interference over the US in *Aqua* AMSR-E data. *IEEE Trans. Geosci. Remote Sens.,* **42,** 380–390, doi:10.1109/TGRS.2003.817195.

Liu, Y. Y., W. A. Dorigo, R. M. Parinussa, R. A. M. de Jeu, W. Wagner, M. F. McCabe, J. P. Evans, and A. I. J. M. van Dijk, 2012: Trend-preserving blending of passive and active microwave soil moisture retrievals. *Remote Sens. Environ.,* **123,** 280–297, doi:10.1016/j.rse.2012.03.014.

Loew, A., T. Holmes, and R. de Jeu, 2009: The European heat wave 2003: Early indicators from multisensoral microwave remote sensing? *J. Geophys. Res.,* **114,** D05103, doi:10.1029/2008JD010533.

Meesters, A. G. C. A., R. A. M. de Jeu, and M. Owe, 2005: Analytical derivation of the vegetation optical depth from the microwave polarization difference index. *IEEE Trans. Geosci. Remote Sens.,* **2,** 121–123, doi:10.1109/LGRS.2005.843983.

Miralles, D. G., and Coauthors, 2014: El Niño–La Niña cycle and recent trends in continental evaporation. *Nat. Climate Change.,* **4,** 122–126, doi:10.1038/nclimate2068.

Naeimi, V., K. Scipal, Z. Bartalis, S. Hasenauer, and W. Wagner, 2009: An improved soil moisture retrieval algorithm for ERS and METOP scatterometer observations. *IEEE Trans. Geosci. Remote Sens.,* **47,** 1999–2013, doi:10.1109/TGRS.2008.2011617.

Njoku, E. G., T. J. Jackson, V. Lakshemi, T. K. Chan, and S. V. Nghiem, 2003: Soil moisture retrieval from AMSR-E. *IEEE Trans. Geosci. Remote Sens.,* **41,** 215–229, doi:10.1109/TGRS.2002.808243.

Oliva, R., E. Daganzo-Eusebio, Y. Kerr, S. Mecklenburg, S. Nieto, P. Richauma, and C. Gruhier, 2012: SMOS radio frequency interference scenario: Status actions taken to improve the RFI environment in the 1400–1427 MHz passive band. *IEEE Trans. Geosci. Remote Sens.,* **50,** 1427–1438, doi:10.1109/TGRS.2012.2182775.

Owe, M., R. de Jeu, and T. Holmes, 2008: Multisensor historical climatology of satellite-derived global land surface moisture. *J. Geophys. Res.,* **113,** F01002, doi:10.1029/2007JF000769.

Parinussa, R. M., T. R. H. Holmes, M. T. Yilmaz, and W. T. Crow, 2011a: The impact of land surface temperature on soil moisture anomaly detection from passive microwave observations. *Hydrol. Earth Syst. Sci.,* **15,** 3135–3151, doi:10.5194/hess-15-3135-2011.

——, A. G. C. A. Meesters, Y. Y. Liu, W. A. Dorigo, W. Wagner, and R. A. M. de Jeu, 2011b: Error estimates for near-real-time satellite soil moisture as derived from the land parameter retrieval model. *IEEE Geosci. Remote Sens. Lett.,* **8,** 779–783, doi:10.1109/LGRS.2011.2114872.

——, T. R. H. Holmes, and R. A. M. de Jeu, 2012: Soil moisture retrievals from the WindSat polarimetric microwave radiometer. *IEEE Trans. Geosci. Remote Sens.,* **50,** 2683–2694, doi:10.1109/TGRS.2011.2174643.

——, M. T. Yilmaz, M. C. Anderson, C. R. Hain, and R. A. M. de Jeu, 2014: An intercomparison of remotely sensed soil moisture products at various spatial scales over the Iberian Peninsula. *Hydrol. Processes,* **28,** 4865–4876, doi:10.1002/hyp.9975.

Rebel, K. T., R. A. M. de Jeu, P. Ciais, N. Viovy, S. L. Piao, G. Kiely, and A. J. Dolman, 2012: A global analysis of soil moisture derived from satellite observations and a land surface model. *Hydrol. Earth Syst. Sci.,* **16,** 833–847, doi:10.5194/hess-16-833-2012.

Reichle, R., and R. Koster, 2004: Bias reduction in short records of satellite soil moisture. *Geophys. Res. Lett.,* **31,** L19501, doi:10.1029/2004GL020938.

Scipal, K., T. R. H. Holmes, R. A. M. de Jeu, V. Naeimi, and W. Wagner, 2008: A possible solution for the problem of estimating the error structures of global soil moisture data sets. *Geophys. Res. Lett.,* **35,** L24403, doi:10.1029/2008GL035599.

Seto, S., N. Takahashi, and T. Iguchi, 2005: Rain/no-rain classification methods for microwave radiometer observations over land using statistical information for brightness temperatures under no-rain conditions. *J. Appl. Meteor.,* **44,** 1243–1259, doi:10.1175/JAM2263.1.

Taylor, C. M., R. A. M. de Jeu, F. Guichard, P. P. Harris, and W. A. Dorigo, 2012: Afternoon rain more likely over drier soils. *Nature,* **489,** 423–426, doi:10.1038/nature11377.

Wagner, W., V. Naeimi, K. Scipal, R. A. M. de Jeu, and J. Martinez Fernandez, 2007: Soil moisture from operational meteorological satellites. *Hydrogeol. J.,* **15,** 121–131, doi:10.1007/s10040-006-0104-6.

——, W. A. Dorigo, R. A. M. de Jeu, D. Fernandez-Prieto, J. Benveniste, E. Haas, and M. Ertl, 2012: Fusion of active and passive microwave observations to create an Essential Climate Variable data record on soil moisture. *Proc. XXII ISPRS Congress,* Melbourne, Australia, ISPRS, 315–321. [Available online at www.isprs-ann-photogramm-remote-sens-spatial-inf-sci.net/I-7/315/2012/isprsannals-I-7-315-2012.pdf.]

Wanders, N., D. Karssenberg, M. F. P. Bierkens, R. M. Parinussa, R. A. M. de Jeu, J. C. van Dam, and S. M. de Jong, 2012: Observation uncertainty of satellite soil moisture products determined with physically based modeling. *Remote Sens. Environ.,* **127,** 341–356, doi:10.1016/j.rse.2012.09.004.

——, M. F. P. Bierkens, S. M. de Jong, A. de Roo, and D. Karssenberg, 2014a: The benefits of using remotely sensed soil moisture in parameter identification of large-scale hydrological models. *Water Resour. Res.,* **50,** 6874–6891, doi:10.1002/2013WR014639.

——, D. Karssenberg, A. de Roo, S. M. de Jong, and M. F. P. Bierkens, 2014b: The suitability of remotely sensed soil moisture for improving operational flood forecasting. *Hydrol. Earth Syst. Sci.,* **18,** 2343–2357, doi:10.5194/hess-18-2343-2014.